Ω and ϕ in Au + Au collisions at $\sqrt{s_{\mathrm{NN}}} = 200$ and 11.5 GeV from a multiphase transport model [*]

Y. J. Ye(叶永金)[1,2]   J. H. Chen(陈金辉)[1;1)]   Y. G. Ma(马余刚)[1,3;2)]   S. Zhang(张松)[1]   C. Zhong(钟晨)[1]

[1] Shanghai Institute of Applied Physics, Chinese Academy of Sciences, Shanghai 201800, China
[2] University of Chinese Academy of Sciences, Beijing 100049, China
[3] ShanghaiTech. University, Shanghai 200031, China

Abstract: Within the framework of a multiphase transport model, we study the production and properties of Ω and ϕ in Au + Au collisions with a new set of parameters for $\sqrt{s_{\mathrm{NN}}} = 200$ GeV and with the original set of parameters for $\sqrt{s_{\mathrm{NN}}} = 11.5$ GeV. The AMPT model with string melting provides a reasonable description at $\sqrt{s_{\mathrm{NN}}} = 200$ GeV, while the default AMPT model describes the data well at $\sqrt{s_{\mathrm{NN}}} = 11.5$ GeV. This indicates that the system created at top RHIC energy is dominated by partonic interactions, while hadronic interactions become important at lower beam energy, such as $\sqrt{s_{\mathrm{NN}}} = 11.5$ GeV. The comparison of $N(\Omega^+ + \Omega^-)/[2N(\phi)]$ ratio between data and calculations further supports the argument. Our calculations can generally describe the data of nuclear modification factor as well as elliptic flow.

Keywords: multi-strangeness particles, AMPT, RHIC

PACS: 25.70.-q, 25.75.Nq   **DOI:** 10.1088/1674-1137/41/8/084101

1 Introduction

Lattice QCD calculations predict a critical point which separates a first-order phase transition and a smooth crossover in the QCD phase diagram [1, 2]. Experimental efforts have been made to explore this at the Relativistic Heavy Ion Collider (RHIC) at BNL, in a dedicated Beam Energy Scan program. Exciting results for QCD matter, including antimatter nuclei detection and its interaction measurement [3–7], non-monotonic behaviour of conserved quantity fluctuation [8–12], and strangeness enhancement [13, 14], have displayed many interesting features. Chiral electromagnetic effects have demonstrated rich phenomena for QCD matter in relativistic heavy-ion collisions [15–17]. Also, the increasing difference between elliptic flows of particles and antiparticles, thus breaking the constituent quark scaling of elliptic flow, has been observed as the collision energy decreases [18] and might be related to phase transition [19–21]. Among these measurements, one of the new ideas is to study the Ω/ϕ ratio in a broad energy range to search for a phase transition signal from a partonic degree of freedom (d.o.f) dominated system to a hadronic interaction dominated system [22]. The transverse momentum

(p_{T}) dependent Ω/ϕ ratio was observed to fall with a consistent trend at high collision energies, but starts to deviate in peripheral collisions at $\sqrt{s_{\mathrm{NN}}} = 19.6$, 27, and 39 GeV, and in central collisions at 11.5 GeV in the intermediate p_{T} region of 2.4−3.6 GeV/c [23] in measurements by the RHIC-STAR collaboration [24–26]. Also, the number of constituent quark scaled Ω/ϕ ratios show a suppression of strange quark production in central collisions at $\sqrt{s_{\mathrm{NN}}} = 11.5$ GeV in comparison with those at $\sqrt{s_{\mathrm{NN}}} \geq 19.6$ GeV [23]. The data indicates that there is likely a change of the underlying strange quark dynamics in the transition from quark matter to hadronic matter at collision energies below 19.6 GeV. However, understanding of the detailed transport dynamics is still missing. In this paper, we study the production of Ω and ϕ at $\sqrt{s_{\mathrm{NN}}} = 200$ and 11.5 GeV by a multiphase transport (AMPT) model with new tuned input parameters.

This article is organized as follows. In Section 2, we introduce the AMPT model in brief and discuss the parameters in the model which are relevant to the p_{T} spectra shapes of identified particles. We present the updated calculation on Ω and ϕ spectra, the particle ratio, the nuclear modification factor and the elliptic flow in Section 3. Finally, a summary is given in Section 4.

2   The AMPT model

The AMPT model has been used extensively to describe the dynamics of system evolution created in high energy heavy-ion collisions [27]. The default version of the AMPT model has four parts: fluctuating initial conditions from the HIJING model [28], the elastic parton cascade from ZPC [29] for minijet partons, the Lund string model [30] for hadronization, and the ART [31] for hadron transport. It describes the rapidity distributions and transverse momentum spectra in heavy-ion collisions from SPS to RHIC energies reasonably well but underestimates the elliptic flow observed at RHIC [27]. It was pointed out by the authors of the model that most of the energy produced in the overlapping volume of heavy-ion collisions are in hadronic strings and are thus not included in the parton cascade in the default AMPT model [32]. A string melting version of the AMPT was then developed, where all excited hadronic strings in the overlap volume are converted into partons [32]. The AMPT model with the string melting scenario consists of fluctuating initial conditions from the HIJING model [28], the elastic parton cascade ZPC [29] for all partons from the melting of hadronic strings, a quark coalescence model based on the quark spatial information for hadronization, and the ART hadronic cascade [31]. Since all hadronic strings in HIJING are converted to partons in the melting version, the parton density in ZPC is quite dense and it can reasonably fit the elliptic flow in heavy-ion collisions at RHIC energy [27]. However, it fails to reproduce the rapidity distributions and the $p_{\rm T}$ spectra well when the same Lund a and b parameters are used as in the default version.

In previous studies, it was found that the multiplicity of charged particles measured in heavy ion collisions at RHIC energy and at LHC energy could be described well by the melting AMPT model with modified parameters of a and b in the Lund string fragmentation function [33, 34]

$$f(z) \propto z^{-1}(1-z)^a \exp(-bm_\perp^2/z), \qquad (1)$$

where z is the light-cone momentum fraction of the produced hadron with respect to that of the fragmenting string. The average square transverse momentum is then given by [27]

$$<p_\perp^2> = \frac{\int p_\perp^2 f(z)d^2p_\perp \mathrm{d}z}{\int f(z)d^2p_\perp \mathrm{d}z}. \qquad (2)$$

For massless particles, it reduces to [27]

$$<p_\perp^2> = \frac{1}{b(2+a)}. \qquad (3)$$

Recently, a systematic study of predictions for $\sqrt{s_{\rm NN}}$ =5.02 TeV Pb+Pb collisions was updated by the same authors with new tuned parameters [35]. Here we tune the parameters in the model to study the dynamics of Ω and ϕ production in Au+Au collisions at $\sqrt{s_{\rm NN}}$= 200 and 11.5 GeV.

Table 1 lists the parameters used in previous studies and the present work. Parameter set B provides a better description of transverse momentum spectra of charged particles at RHIC energy than set A does for p+p and d + Au data [36], though both give a softer spectrum than experimental data. We here tune the parameters again to try to match the data. In particular, we apply a small parton cascade cross section of 1.5 mb in comparison with the parameter sets of 3 mb as discussed in Ref. [35]. According to Eq. (3), we know that the parameters a and b determine the $p_{\rm T}$ distribution of particle production. A large a and b will give a small average square transverse momentum distribution, which will give a sharp $p_{\rm T}$ spectrum, while small a and b will give a flat distribution. In the study of the Lund string fragmentation model in the AMPT [37], we also know that quark-antiquark pair production probability is proportional to $\exp(-\pi m_\perp^2/\kappa)$, where κ is the string tension and $\kappa \propto \frac{1}{b(a+2)}$. Due to its large mass, strange quark production is suppressed by the factor $\exp(-\pi(m_s^2-m_u^2)/\kappa)$, compared to that of light quarks. So, larger values of a and b lead to a suppression of strangeness.

Table 1.   Values of $\boldsymbol{a}$ and $\boldsymbol{b}$ in the Lund string fragmentation function and α_s, μ relevant to the parton scattering cross section via $\sigma \approx 9\pi\alpha_s^2/(2\mu^2)$. Set A [27] and Set B [33] are from previous studies, and Set C is the present work.

	$\boldsymbol{a}$	$\boldsymbol{b}$/GeV^{-2}	α_s	μ/fm^{-1}
A	2.2	0.5	0.47	1.8
B	0.5	0.9	0.33	3.2
C	0.55	0.15	0.33	3.2

Figure 1 shows the transverse momentum spectra of charged π and $\bar{p}$ in Au+Au collisions at $\sqrt{s_{\rm NN}} = 200$ GeV from the string melting AMPT model (version 2.26t5 for this study, available online [38]). The result at $\sqrt{s_{\rm NN}}$ = 11.5 GeV from the default AMPT model is presented in panel (b). In panel (a), it is seen that all parameter sets describe the experimental data [39] reasonably well at low $p_{\rm T}$. At high $p_{\rm T}$, parameter set C gives larger yields as a result of smaller energy loss of high $p_{\rm T}$ particles when the parton scattering cross section is smaller for parameter set C (1.5 mb) than parameter set A (10 mb). Parameter set C gives flatter $p_{\rm T}$ spectra than parameter sets A and B because of the smaller values of a and b, which dominate the charged particle $p_{\rm T}$ spectra as mentioned before. Parameter set C describes the experimental data well, and a smaller b will reduce the suppression of strangeness, which relates to our study in this paper. So we choose parameter set C at energy

$\sqrt{s_{NN}} = 200$ GeV, while keeping parameter set A at energy $\sqrt{s_{NN}} = 11.5$ GeV due to the strong suppression of strange quark production at lower energy, which will be illustrated by the strange matter p_T spectra in the following discussion. Because the experimental data for $\sqrt{s_{NN}} = 11.5$ GeV is not published yet, panel (b) only shows our calculation, and the comparison with experimental data is not involved. The transverse momentum spectra for charged π and $\bar{p}$ show similar features for the AMPT model with the three different parameter sets at 200 GeV (panel a).
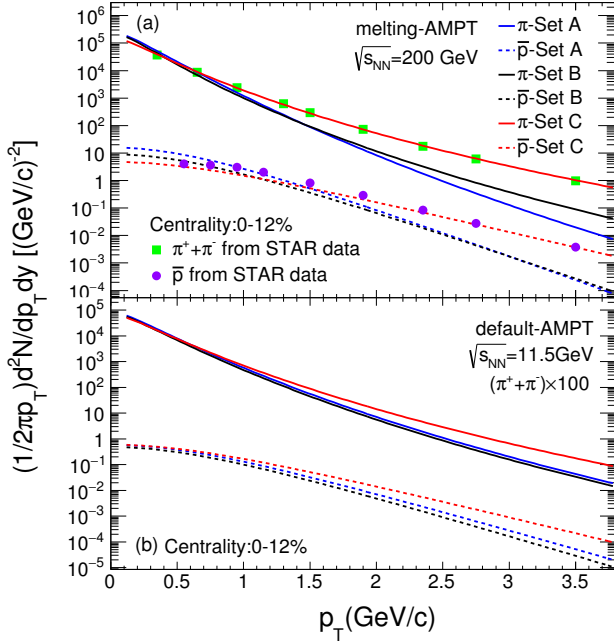

Fig. 1.   (color online) The π and $\bar{p}$ invariant yields as a function of p_T in Au+Au collisions. (a) Calculations of the AMPT model with the string melting scenario for $\sqrt{s_{NN}} = 200$ GeV with different parameter sets A, B and C. The experimental data [39] are also plotted for comparison. (b) Calculations from the default AMPT model at $\sqrt{s_{NN}} = 11.5$ GeV.

3   Results

3.1   Production of Ω and ϕ

The Ω and ϕ invariant yields as a function of p_T in Au+Au collisions from the AMTP model are shown in Figure 2. The upper panel shows the yields of Ω and ϕ at $\sqrt{s_{NN}}=200$ GeV. For the ϕ meson, the rapidity range is $|y| < 1.0$, while for the Ω, the rapidity range is $|y|<0.75$, the same window as the experimental analysis. The AMPT model with the string melting scenario describes the production of the ϕ meson well at energy $\sqrt{s_{NN}} = 200$ GeV [40], while the default version gives a

small deviation in the slope of the ϕ meson p_T spectrum in comparison with data. Both AMPT with string melting and the default version describe the slope of the Ω spectra and underpredict the rate by a factor of 5.0 [41], which may be due to the current coalescence algorithm in the AMPT model, which shows the algorithm or model can be further improved in future [27].
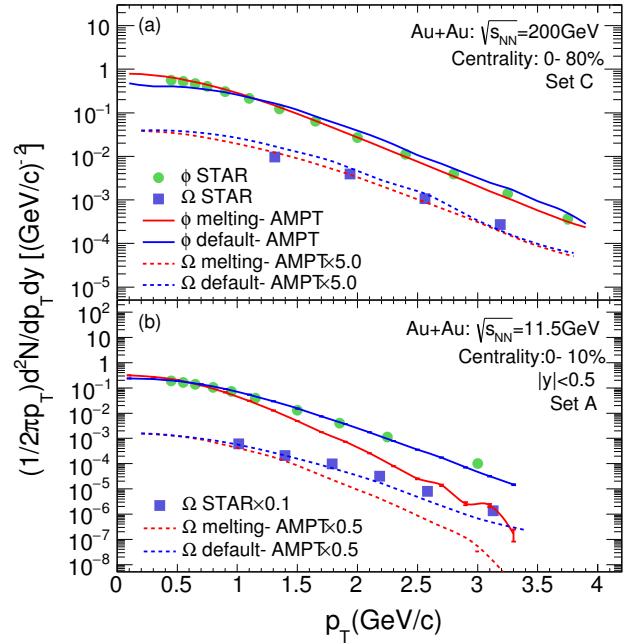

Fig. 2.   (color online) The invariant yields of Ω baryon and ϕ meson as a function of p_T in Au+Au collisions at (a) $\sqrt{s_{NN}} = 200$ GeV and (b) $\sqrt{s_{NN}} = 11.5$ GeV. The calculations are compared with experimental data and different sets of parameters are used.

Moving to the lower energy, as shown in Fig. 2(b), the default AMPT model describes the ϕ meson data well [23], while the melting AMPT model describes the data at low p_T but underpredicts the production rate significantly at high p_T. This is probably due to the fact that the AMPT model with string melting scenario includes significant parton interactions, which leads to a larger energy loss when the partons pass through the medium before hadronization than with the default AMPT. For the Ω, the AMPT model with the default scenario describes the experimental data well after the yield of Ω is scaled by a factor 5.0. The production rate is strongly suppressed at high p_T in the AMPT with the string melting scenario and deviates from the experimental data. A comparison between panel (a) and panel (b) indicates that parton interactions are important in Au + Au collisions at $\sqrt{s_{NN}} = 200$ GeV, while hadronic interactions become important at $\sqrt{s_{NN}} = 11.5$ GeV. This is consistent with the findings on possible partonic dom-

inated d.o.f to hadronic dominated d.o.f from the RHIC BES analysis for Ω and ϕ production [23].

3.2   Strangeness dynamics in the system evolution

A quark recombination model calculation by Hwa and Yang has been established to describe the physics of the ratio of Ω/ϕ invariant yields in Au + Au collisions at $\sqrt{s_{\mathrm{NN}}}$=200 GeV [42]. In their model, if we only consider the thermal contribution, the invariant yield distribution of Ω and ϕ is [42]:

$$\frac{\mathrm{d}N_\Omega}{p\mathrm{d}p}=g_\Omega C_s^3 \frac{p^2}{27p_0}\mathrm{e}^{-\frac{p}{T_s}},\tag{4}$$

$$\frac{\mathrm{d}N_\phi}{p\mathrm{d}p}=g_\phi C_s^2 \frac{p}{4p_0}\mathrm{e}^{-\frac{p}{T_s}},\tag{5}$$

where g_Ω and g_ϕ are statistical factors, and T_s is the inverse slope. C_s is a normalization factor which is adjusted to fit the experimental data at low p, and has the dimension [momentum]$^{-1}$. The Ω/ϕ ratio $R_{\Omega/\phi}$ is then derived:

$$R_{\Omega/\phi}^{th}(p)=\frac{4g_\Omega C_s}{27g_\phi}p\tag{6}$$

From Eq. 6, one can find that the ratio increases linearly as momentum increases if one only considers the thermal contribution.

Figure 3 shows the results from the AMPT model for the ratio of $N(\Omega^++\Omega^-)/[2N(\phi)]$ in Au + Au collisions at mid-rapidity at $\sqrt{s_{\mathrm{NN}}} = 200$ GeV and 11.5 GeV. In Fig. 3(a), one can see that the ratio after the Ω yields from the melting AMPT are scaled by a factor of 5.0 describes the experimental data [23] reasonably well and gives an approximately straight line, but the result from the default AMPT model does not describe the data. At $\sqrt{s_{\mathrm{NN}}} = 11.5$ GeV, as shown in Fig. 3(b), both the default AMPT and the melting AMPT seem to describe the shape of the data with large statistical errors. As we discussed in the previous section, however, the AMPT model with the string melting scenario underpredicts the Ω-baryon and ϕ-meson spectra at high p_{T} even though the ratios seem along the right way [c.f. Fig. 2]. The ratio at $p_{\mathrm{T}} = 0.0$ GeV/c from our calculation is higher than 0, contrary to the expectation from Eq. (6). This may indicate that Hwa and Yang's model works better at intermediate p_{T} where quark coalescence dominates the particle production.

One interesting feature from the comparison of AMPT model calculation with data is that the turning down point of the Ω/ϕ ratio seems to move to lower p_{T} from $\sqrt{s_{\mathrm{NN}}} = 200$ GeV to 11.5 GeV. The Ω and ϕ only contain strange quarks without any light quarks. Thus they are not affected by the light shower partons at high p_{T}, and their production will be dominated by thermal strange quark recombination. In the AMPT model with

string melting, the coalescence model is involved, where the hadrons combine from the deconfined quarks after sufficient parton interaction. The assumption from Hwa and Yang [42] is consistent with the coalescence model in the AMPT model. For the default AMPT model, the quark combined with the parent string does not have sufficient interaction from the partonic stage, so the turning point of the ratio is lower.
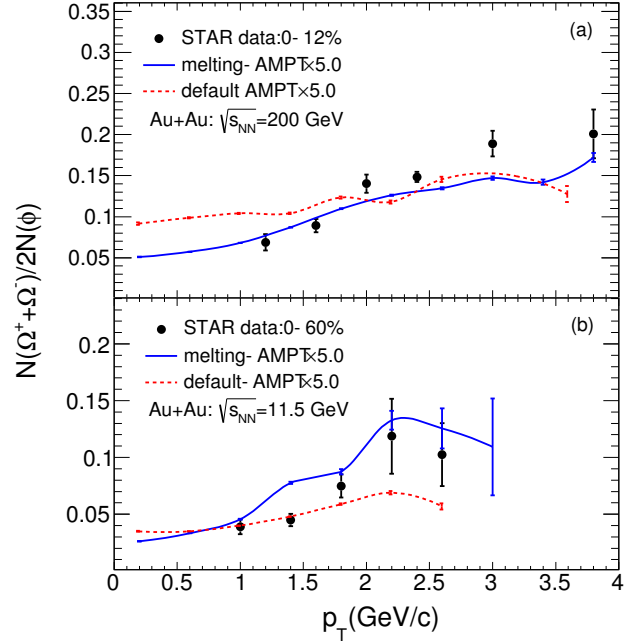

Fig. 3. (color online) The ratio of $N(\Omega^+ + \Omega^-)/[2N(\phi)]$ as a function of p_{T} in Au + Au collisions. (a) AMPT model calculation with the string melting version at $\sqrt{s_{\mathrm{NN}}} = 200$ GeV (parameter set C) and (b) default AMPT model calculation at $\sqrt{s_{\mathrm{NN}}} = 11.5$ GeV (parameter set A).

To investigate the strangeness dynamics in more detail, we compare the strange quark transverse momentum distribution after partonic interaction ceases in the AMPT model with the ratio of $\dfrac{N(\Omega^-+\Omega^+)|_{p_{\mathrm{T}}^\Omega=3p_{\mathrm{T}}^s}}{2N(\phi)|_{p_{\mathrm{T}}^\phi=2p_{\mathrm{T}}^s}}$ from final state hadrons. In the framework of quark coalescence/recombination, the Ω baryons are formed from the coalescence of three strange quarks of approximately equal momentum, and the ϕ meson is from a strange quark and an anti-strange quark. Under this logic, the production of Ω baryons is proportional to the local strange quark density, $f_s^3(p_{\mathrm{T}}^s)$, and the yield of ϕ mesons is proportional to $f_s(p_{\mathrm{T}}^s)f_{\bar{s}}(p_{\mathrm{T}}^{\bar{s}})$, where $f_s(f_{\bar{s}})$ is the strange (anti-strange) quark p_{T} distribution at hadronization. If we take the approximation that f_s is equal to $f_{\bar{s}}$, then the ratio $\dfrac{N(\Omega^-+\Omega^+)|_{p_{\mathrm{T}}^\Omega=3p_{\mathrm{T}}^s}}{2N(\phi)|_{p_{\mathrm{T}}^\phi=2p_{\mathrm{T}}^s}}$ is proportional to $f_s(p_{\mathrm{T}}^s)$. Figure 4 shows the NCQ-scaled

$\dfrac{N(\Omega^- + \Omega^+)|_{p_T^\Omega = 3p_T^s}}{2N(\phi)|p_T^\phi = 2p_T^s}$ ratios and the production of strange quarks at hadronization (scaled by an appropriate factor) as a function of $p_T^s = p_T/n_q$ at mid-rapidity ($|y| < 0.5$) from central Au + Au collisions at $\sqrt{s_{\text{NN}}} = 200$ GeV. The NCQ-scaled ratio from the AMPT model describes the experimental data reasonably well. The production of strange quarks at hadronization after being scaled by an appropriate factor is consistent with the NCQ-scaled ratio, which is a further confirmation of the coalescence assumption. This consistency also reflects the small influence of the production of Ω and ϕ during final state interaction of hadrons by comparing the distribution from the melting-AMPT model with the ZPC model with parameter set C. In this way, the strange quark p_T distribution at hadronization from parameter set C gives a better description of the experimental data than parameter set A. Therefore, the AMPT model with parameter set C provides a good description of the strange quark production in Au + Au collisions at $\sqrt{s_{\text{NN}}} = 200$ GeV.
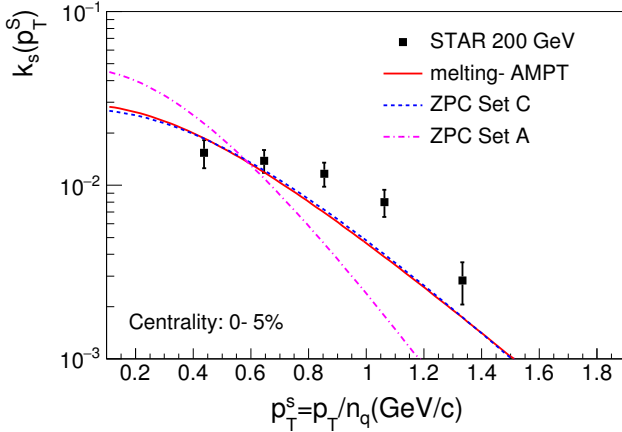

Fig. 4.   (color online) The NCQ-scaled $N(\Omega^+ + \Omega^-)/[2N(\phi)]$ ratio ($k_s(p_T^s)$) at midrapidity ($|y| < 0.5$) as a function of p_T per constituent quark for central Au + Au collisions at $\sqrt{s_{\text{NN}}} = 200$ GeV. The solid line represents the AMPT model result. The dashed and dash-dotted lines are the strange quark p_T distributions in AMPT from the ZPC. Experimental data [23] are also plotted for comparison.

3.3 Nuclear modification factor

The centrality ratio of the p_T spectrum scaled by the number of binary nucleon-nucleon collisions (N_{bin}) is a measure of the particle production dependence on the collisions system size and density [43]:

$$R_{\text{CP}} = \frac{[dN/dp_T/N_{\text{bin}}]^{\text{Central}}}{[dN/dp_T/N_{\text{bin}}]^{\text{Peripheral}}}, \qquad (7)$$

where $R_{\text{CP}} = 1$ if particle production is equivalent to a superposition of independent nucleon-nucleon collisions,

and other values illustrate the medium effect. Figure 5 presents the R_{CP} result in the AMPT model. The collision centrality interval in $\sqrt{s_{\text{NN}}} = 200$ GeV and 11.5 GeV is chosen differently to match the experimental data at each energy [23, 40]. At $\sqrt{s_{\text{NN}}} = 200$ GeV, the R_{CP} values of both ϕ and Ω are all smaller than 1 and suppressed at high p_T. At $\sqrt{s_{\text{NN}}} = 11.5$ GeV, the R_{CP} of the ϕ meson is close to 1 and the $R_{\text{CP}}(p_T)$ of Ω is similar to that of the ϕ, though with large statistical uncertainty. The large centrality interval of peripheral collisions (10%–60%) at $\sqrt{s_{\text{NN}}} = 11.5$ GeV is mainly due to the limited statistics and small cross section for the Ω baryon. In comparison with the data, the AMPT model calculation at $\sqrt{s_{\text{NN}}} = 200$ GeV gives a correct trend of suppression at higher p_T even though the quantity is underestimated for ϕ-mesons, which needs to be further improved to describe the whole centrality dependence. For 11.5 GeV, our model calculations can essentially describe the data well.
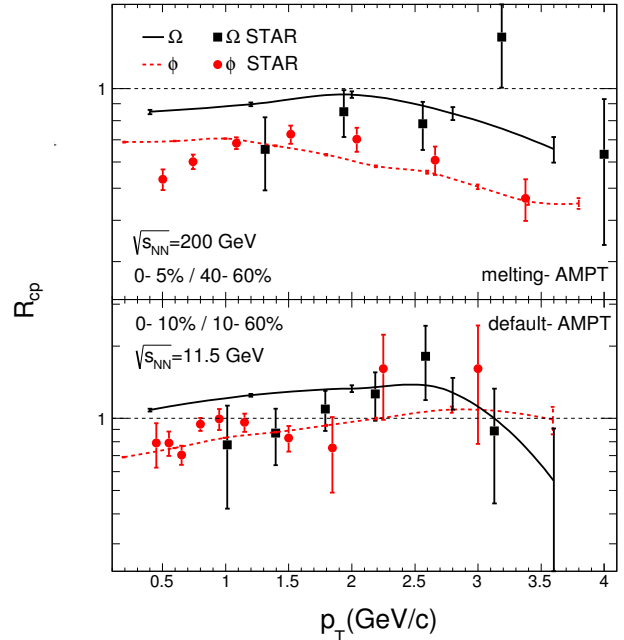

Fig. 5.   (color online) The nuclear modification factor (R_{CP}) of Ω and ϕ as a function of p_T in Au+Au collisions. (a) AMPT model calculation with the string melting version at $\sqrt{s_{\text{NN}}} = 200$ GeV (parameter set C) and (b) default AMPT model calculation at $\sqrt{s_{\text{NN}}} = 11.5$ GeV (parameter set A). The experimental data [23, 40] from the STAR Collaboration are plotted for comparison.

3.4 Elliptic flow of Ω and ϕ

We further study the elliptic flow of Ω and ϕ with our new tuned parameters. In previous work, we learned that the AMPT model calculation in Au + Au collisions at $\sqrt{s_{\text{NN}}} = 200$ GeV with parameter set A describes the

charged particle elliptic flow well at intermediate $p_{\rm T}$ but overestimates the magnitude by 25% in the low $p_{\rm T}$ region [44].

Elliptic flow is one of the important probes of collective dynamics in heavy ion reactions [45]. It results from the spatial asymmetry in the transverse plane in non-central collisions, which is larger at early times. Therefore, the elliptic flow is sensitive to the properties of dense matter, such as the cross section of partons produced in collisions [46–49] or its equation of state [50–53]. Measurements of elliptic flow in Au + Au collisions at RHIC give us much knowledge of the partonic interaction strength and the effective energy loss of partons [54–56].
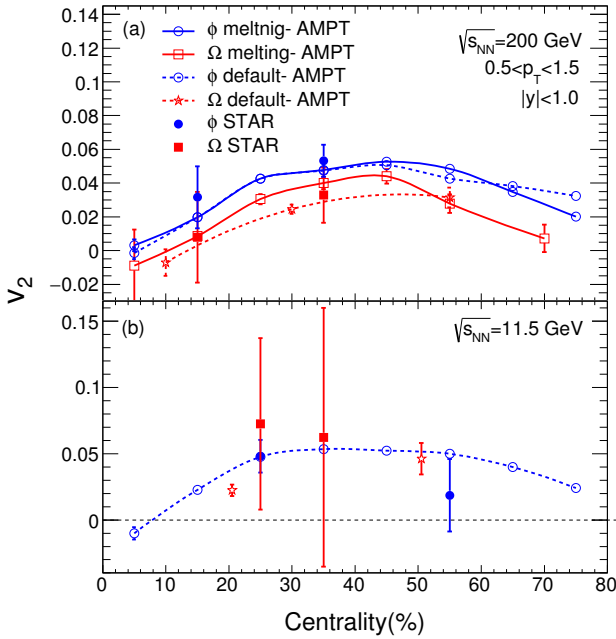

Fig. 6.   (color online) Elliptic flow of Ω and ϕ versus collision centrality in Au + Au collisions at RHIC. (a) AMPT model calculation at $\sqrt{s_{\rm NN}}$=200 GeV (parameter set C) and (b) default AMPT model calculation at $\sqrt{s_{\rm NN}}$ = 11.5 GeV (parameter set A). Experimental data are also plotted for comparison [54–56].

Figure 6(a) shows the elliptic flow of Ω and ϕ in Au + Au collisions at $\sqrt{s_{\rm NN}}$ = 200 GeV in broad centrality intervals. The elliptic flow of ϕ increases from central collision to peripheral collision up to 40%–50% and then decreases from 50%−80%. The centrality dependence of the Ω elliptic flow from the AMPT model is similar to that of the ϕ. In comparison with the data, the AMPT model with the new tuned parameters perfectly describes the low $p_{\rm T}$ Ω and ϕ v_2 in both magnitude and centrality

dependence. The difference between default and melting AMPT is small and future accurate data will help to distinguish the calculation. Figure 6(b) presents the elliptic flow from the default AMPT model at $\sqrt{s_{\rm NN}}$=11.5 GeV. Because of the lower rate of strangeness production at $\sqrt{s_{\rm NN}}$=11.5 GeV, the statistical error is large both from simulation and experimental data.

4   Summary

Multi-strange particles, namely ϕ and Ω, have been studied in Au + Au collisions at RHIC in a multiphase transport model. Firstly, a new set of parameters (set C) has been adopted in the AMPT model, and provides us with a relatively accurate description of the production of π and $\bar{p}$ invariant yields at $\sqrt{s_{\rm NN}} = 200$ GeV. Secondly, the transverse momentum spectra of Ω and ϕ have been presented. The AMPT model with the string melting scenario describes the experimental data well at $\sqrt{s_{\rm NN}} = 200$ GeV, while the default AMPT model provides a good description at $\sqrt{s_{\rm NN}}$=11.5 GeV. However, we need to remember that the Ω yield is still underestimated by a factor of 5 even though the new set of parameters is used. It indicates future improvement of the model or coalescence mechanism is needed. The parton interaction is dominant in Au + Au collisions at $\sqrt{s_{\rm NN}} = 200$ GeV and the interaction strength becomes weak in collisions at $\sqrt{s_{\rm NN}} = 11.5$ GeV. The argument is further supported by the study of the ratio of $N(\Omega^{+}+\Omega^{-})/[2N(\phi)]$ versus transverse momentum. The deconfined quarks are involved at $\sqrt{s_{\rm NN}}$=200 GeV in the melting AMPT model, which leads to a linear increase of the ratio, and is in good agreement with other recombination model calculations [42]. The $N(\Omega^{+}+\Omega^{-})/[2N(\phi)]$ ratio is proportional to the strange quark density, which provides more support for the assumption of the coalescence model. The value of the $N(\Omega^{+}+\Omega^{-})/[2N(\phi)]$ ratio turns down at lower $p_{\rm T}$ from $\sqrt{s_{\rm NN}} = 200$ GeV to 11.5 GeV, which indicates the transition from partonic-dominated to hadronic-dominated dynamics as shown by the experimental data [23]. Our calculations also give a reasonable description of the nuclear modification factor data for Au + Au collisions at $\sqrt{s_{\rm NN}} = 200$ GeV and 11.5 GeV using the melting AMPT and default AMPT, respectively. Elliptic flows of Ω and ϕ can describe the experimental data well at low $p_{\rm T}$ with the new parameter set. In the future, the STAR experiment will accumulate large datasets for Au + Au collisions over a range of beam energies during 2019 and 2020 Beam Energy Scan Phase-II runs, which will further improve the precision of the Ω and ϕ measurements and will likely provide new insight into the effective degrees of freedom of the system created at RHIC.

References

1 Y. Aoki, G. Endrodi, Z. Fodor, S. D. Katz, and K. K. Szabo, Nature, **443**: 675 (2006)
2 F. Karsch, Prog. Theor. Phys. Suppl., **168**: 237 (2007)
3 B. I. Abelev et al (STAR Collaboration), Science, **328**: 58 (2010)
4 B. I. Abelev et al (STAR Collaboration), Nature, **473**: 353 (2011)
5 For a review paper, see eg., Yu-Gang Ma, Jin-Hui Chen, and Liang Xue, Front. Phys., **7**: 637 (2012)
6 L. Adamczyk et al (STAR Collaboration), Nature, **527**: 345 (2015)
7 Z. Q. Zhang and Y. G. Ma, Nucl. Sci. Tech., **27**: 152 (2016)
8 L. Adamczyk et al (STAR Collaboration), Phys. Rev. Lett., **112**: 032302 (2014)
9 L. Adamczyk et al (STAR Collaboration), Phys. Rev. Lett., **113**: 092301 (2014)
10 L. Adamczyk et al (STAR Collaboration), Phys. Rev. C, **92**: 021901(R) (2015)
11 C. M. Ko, F. Li, Nucl. Sci. Tech., **27**: 140 (2016)
12 For a review paper, see eg., X. F. Luo and N. Xu, Nucl. Sci. Tech., **28**: in press (2017)
13 S. V. Afanasiev et al (NA49 Collaboration), Phys. Rev. C, **66**: 054902 (2002)
14 C. Alt et al (NA49 Collaboration), Phys. Rev. C, **77**: 024903 (2008)
15 D. E. Kharzeev, L. D. McLerran, and H. J. Warringa, Nucl. Phys. A, **803**: 227 (2008)
16 For a review paper, see eg., K. Hattori and X. Huang, Nucl. Sci. Tech., **28**: 26 (2017)
17 G. L. Ma and X. G. Huang, Phys. Rev. C, **91**: 054901 (2015)
18 L. Adamczyk et al (STAR Collaboration) , Phys. Rev. Lett., **110**: 142301 (2013)
19 J. Tian, J. H. Chen, Y. G. Ma et al: Phys. Rev. C, **79**: 067901 (2009)
20 J. Xu, T. Song, C. M. Ko, and F. Li, Phys. Rev. Lett., **112**: 012301 (2014)
21 C. M. Ko et al, Nucl. Sci. Tech., **24**: 050525 (2013)
22 J. H. Chen, F. Jin, D. Gangadharan, X. Z. Cai, H. Z. Huang, and Y. G. Ma, Phys. Rev. C, **78**: 034907 (2008)
23 L. Adamczyk, et al (STAR Collaboration), Phys. Rev. C, **93**: 021903(R) (2016)
24 K. Ackermann et al. (STAR Collaboration), Nucl. Instrum. Methods A, **499**: 624 (2003)
25 Y. F. Xu, Y. J. Ye, J. H. Chen, Y. G. Ma, S. Zhang, and C. Zhong, Nucl. Sci. Tech., **27**: 87 (2016)
26 L. Ma, X. Dong, H. Qiu, S. Margetis, and Y. G. Ma, Nucl. Sci. Tech., **28**: 25 (2017)

27 Z. W. Lin, C. M. Ko, B. A. Li, B. Zhang, and S. Pal, Phys. Rev. C, **72**: 064901 (2005)
28 X. N. Wang and M. Gyulassy, Phys. Rev. D, **44**: 3501 (1991); M. Gyulassy and X. N. Wang, Comput. Phys. Commun., **83**: 307 (1994)
29 B. Zhang, Comput. Phys. Commum., **109**: 193 (1998)
30 B. Andersson, G. Gustafson, G. Ingelman, and T. Sjöstrand, Phys. Rep., **97**: 31 (1983)
31 B. A. Li and C. M. Ko, Phys. Rev. C, **52**: 2037 (1995)
32 Z. W. Lin and C. M. Ko, Phys. Rev. C, **65**: 034904 (2002)
33 J. Xu and C. M. Ko, Phys. Rev. C, **84**: 014903 (2011)
34 Z. W. Lin, Phys. Rev. C, **90**: 014904 (2014)
35 G. L. Ma and Z. W. Lin, Phys. Rev. C, **93**: 054911 (2016)
36 B. I. Abelev et al (STAR Collaboration), Phys. Rev. C, **76**: 064904 (2007)
37 Z. W. Lin, S. Pal, C. M. Ko, B. A. Li, and B. Zhang, Phys. Rev. C, **64**: 011902(R) (2001)
38 http://myweb.ecu.edu/linz/ampt/
39 B. I. Abelev et al (STAR Collaboration), Phys. Lett. B, **655**: 104 (2007)
40 B.I. Abelev et al (STAR Collaboration), Phys. Rev. Lett., **99**: 112301 (2007)
41 J. Adams et al (STAR Collaboration), Phys. Rev. Lett., **98**: 062301 (2007)
42 R. C. Hwa and C. B. Yang, Phys. Rev. C, **75**: 054904 (2007)
43 J. Adams et al (STAR Collaboration), Phys. Rev. Lett., **92**: 052302 (2004)
44 J. H. Chen, Y. G. Ma, and G. L. Ma et al: Phys. Rev. C, **74**: 064902 (2006)
45 For a review paper, see e.g., J. Ollitrault, Nucl. Phys. A, **638**: 195 (1998)
46 Z. W. Lin and C. M. Ko, Phys. Rev. C, **65**: 034904 (2002)
47 B. Zhang, M. Gyulassy, and C. M. Ko, Phys. Lett. B, **455**: 45 (1999)
48 D. Molnar and M. Gyulassy, Nucl. Phys. A, **697**: 495 (2002)
49 E. E. Zabrodin et al, Phys. Lett. B, 508: 184 (2001)
50 P. F. Kolb, J. Sollfrank, and U. W. Heinz, Phys. Lett. B, **459**: 667 (1999); Phys. Rev. C, **62**: 054909 (2000)
51 D. Teaney, J. Lauret, and E. V. Shuryak, Phys. Rev. Lett., **86**: 4783 (2001)
52 P. Huovijnen et al, Phys. Lett. B, **503**: 58 (2001)
53 P. F. Kolb et al, Nucl. Phys., **A696**: 197 (2001)
54 L. Adamczyk et al (STAR Collaboration), Phys. Rev. Lett., **116**: 062301 (2016)
55 L. Adamczyk et al (STAR Collaboration), Phys. Rev. Lett., **99**: 112301 (2007)
56 L. Adamczyk et al (STAR Collaboration), Phys. Rev. C, **93**: 014907 (2016)